Spectrochimica Acta Part A 78 (2011) 1004–1012

Contents lists available at ScienceDirect

Spectrochimica Acta Part A: Molecular and Biomolecular Spectroscopy

journal homepage: www.elsevier.com/locate/saa

ESR, electrochemical, molecular modeling and biological evaluation of 4-substituted and 1,4-disubstituted 7-nitroquinoxalin-2-ones as potential anti-*Trypanosoma cruzi* agents

Benjamín Aguilera-Venegas[a], Claudio Olea-Azar[a,*], Ester Norambuena[b], Vicente J. Arán[c], Fernando Mendizábal[d], Michel Lapier[a], Juan Diego Maya[e], Ulrike Kemmerling[e], Rodrigo López-Muñoz[e]

[a] Departamento de Química Inorgánica y Analítica, Facultad de Ciencias Químicas y Farmacéuticas, Universidad de Chile, Casilla 233, Santiago, Chile
[b] Departamento de Química, Facultad de Ciencias Básicas, Universidad Metropolitana de Ciencias de la Educación, Santiago, Chile
[c] Instituto de Química Médica (CSIC), Juan de la Cierva 3, 28006 Madrid, Spain
[d] Departamento de Química, Facultad de Ciencias, Universidad de Chile, Casilla 653, Santiago, Chile
[e] Departamento de Farmacología Molecular y Clínica, Facultad de Medicina, Universidad de Chile, Santiago, Chile

ARTICLE INFO

Article history:
Received 7 July 2010
Received in revised form 28 October 2010
Accepted 9 December 2010

Keywords:
Nitroquinoxaline
Chagas' disease
ESR
Trypomastigote
Epimastigote
Molecular Modeling

ABSTRACT

Electrochemical and ESR studies were carried out in this work with the aim of characterizing the reduction mechanisms of 4-substituted and 1,4-disubstituted 7-nitroquinoxalin-2-ones by means of cyclic voltammetry in DMSO as aprotic solvent. Two reduction mechanisms were found for these compounds: the first, for compounds bearing a labile hydrogen by following a self-protonation mechanism (ECE steps), and the second, for compounds without labile hydrogen, based on a purely electrochemical reduction mechanism (typical of nitroheterocycles). The electrochemical results were corroborated using ESR spectroscopy allowing us to propose the hyperfine splitting pattern of the nitro-radical, which was later corroborated by the ESR simulation spectra. All these compounds were assayed as growth inhibitors against *Trypanosoma cruzi*: first, on the non-proliferative (and infective) form of the parasite (trypomastigote stage), and then, the ones that displayed activity, were assayed on the non-infective form (epimastigote stage). Thus, we found four new compounds highly active against *T. cruzi*. Finally, molecular modeling studies suggest the inhibition of the trypanothione reductase like one of the possible mechanisms involved in the trypanocidal action.

1. Introduction

American trypanosomiasis (commonly known as Chagas' disease) is one of the fastest growing diseases in Latin America [1], affecting around 20–24 million of people according to the latest reports from WHO. The etiological agent of this pathology is *Trypanosoma cruzi* (kinetoplastida Trypanosomatidae), a protozoan parasite sensitive to the oxidative stress [2]. Because of this sensitivity to the redox unbalance, two drugs are commonly used in the treatment of this pathology: nifurtimox (Nfx) and benznidazole (Bnz). Both drugs exploit the parasite deficiency by generating oxidative damage [3–6]. These compounds show similar efficacies in the acute phase; however, several side effects have been observed in their use [7]. This has led to the retreat of certain drugs from the market [8]. The drugs act by means of an initial bio-reduction of the NO_2 group (but by following different mechanisms of action [9,10]), generating a series of reduced metabolites of high toxicity (superoxide anion, hydrogen peroxide and hydroxyl radical) [11] that triggers the oxidative stress into the parasite. The search of new and better drugs against *T. cruzi* that can improve this property (without these side effects) is of vital significance in the development of new compounds for the treatment of this pathology. Thus, a variety of compounds have been developed with this aim; including 5-nitroindazoles that show interesting *in vitro* biological activity that enhance this property [12–15] (which have also demonstrated its effectiveness in a mammal model of Chagas' disease [16]); some nitrofuryl derivatives [17–19] and a new variety of drugs that show the capability for inhibiting the growth of the parasite through the generation of reactive oxygen species.

Within the variety of compounds currently evaluated, a new family of nitroquinoxalines (Fig. 1) has been assessed *in silico* by means of QSAR studies as trichomonacidals with auspicious results

* Corresponding author. Tel.: +56 2 9782834; fax: +56 2 7370567.
E-mail address: colea@uchile.cl (C. Olea-Azar).

1386-1425/$ – see front matter © 2010 Elsevier B.V. All rights reserved.
doi:10.1016/j.saa.2010.12.017

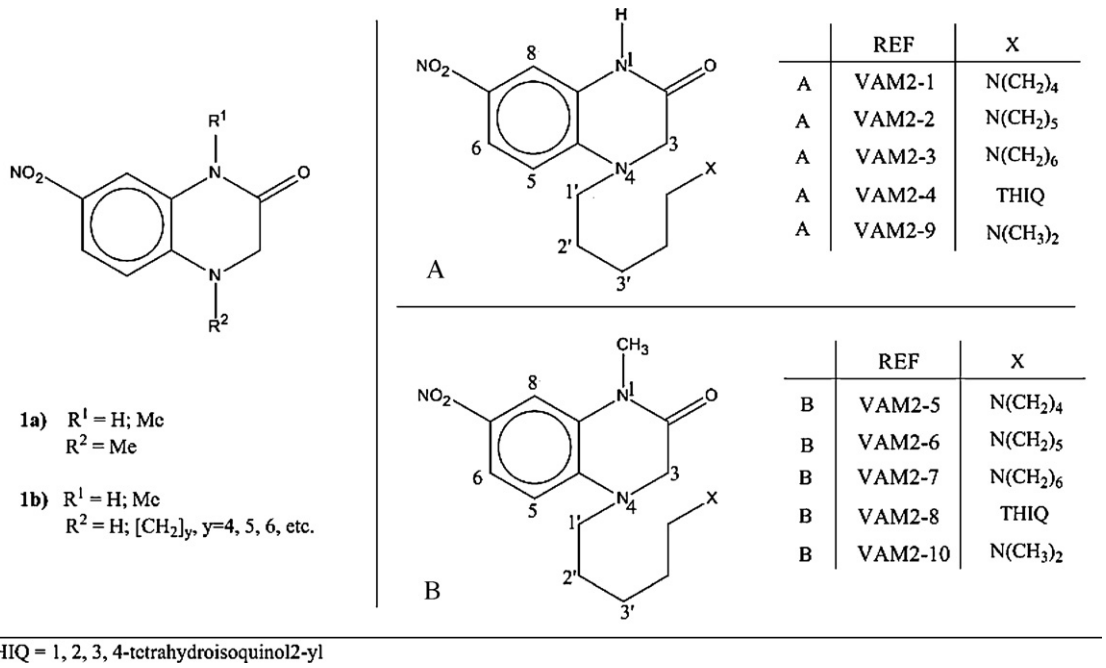

Fig. 1. Chemical structure of the nitroquinoxaline precursors (a) and its derivatives (b). To the right, the 4-substituted and 1,4-disubstituted 7-nitroquinoxalin-2-ones. (A) A series derivatives; (B) B series derivatives.

[20]. Some derivatives such as **1a** (Fig. 1) designed and assessed as potential anti-*Trypanosoma cruzi* and anti-*Trichomonas vaginalis* by showing potential biological activity [21]. Whereby, a new variety of nitro-derivatives (compounds **1b**, Fig. 1) such as: 4-substituted and 1,4-disubstituted 7-nitroquinoxalin-2-ones (A and B series specifically according to our enumeration) have been synthesized [22]. Thus, this paper describes the study of a new family of nitro-heterocycles like potentials agents against *T. cruzi*.

To the best of our knowledge free radicals are species of ephemeral life. They are involved in diverse biological process; in the case of Chagas' disease, the pathway by which they are involved is through an intracellular bio-reduction of the drug (nitro-compound), giving start to the nitro-radical generation, followed by a self-oxidation that triggers a series of reactions that produce a number of reduced subspecies such as oxygen free radicals so toxic to the parasite like to the human. Thus, the nitro-radical acts as initiator of oxidative stress indiscriminately between the parasite and the host (explaining the toxic effects in mammalian host) through the free radical generation, but by means of different action mechanisms, so it is of great interest to the study of the mechanisms of reduction of the different kinds of nitroquinoxalines proposed for this study and the characterization of the radicalary species that could be generated.

The life cycle of *T. cruzi* is extensive and complex that involves an extracellular, proliferative stage (*epimastigote*) that resides in the insect vector, and two forms that occur in the mammalian host: a non-proliferative and infective form (*trypomastigote*) and an intracellular and proliferative form (*amastigote*) [23]. In this work, we assayed the nitroquinoxaline against this protozoan in its infective stage (trypomastigote form), and for compounds capable to inhibit parasite growth (according to the results from the viability assays), further evaluations on the non-infective form of the parasite (epimastigote form) were carried out according to the protocols indicated by Faundez et al. [24].

Thus, the aim of this work was to investigate through electrochemical and ESR spectroscopy in the reduction pathways of 4-substituted and 1,4-disubstituted 7-nitroquinoxalin-2-ones, and assess its effectiveness as anti-protozoan agents, evaluating them as growth inhibitors of *T. cruzi* through several cytotoxicity assays on different growing states of the parasite.

2. Experimental

2.1. Reagents

The 4-substituted and 1,4-disubstituted 7-nitroquinoxalin-2-ones derivatives (A and B series, Fig. 1) were synthesized according to the methods described earlier [22]. Studied compounds: VAM2-1: 7-nitro-4-(5-pyrrolidinopentyl)-3,4-dihydro-1*H*-quinoxalin-2-one hydrobromide; VAM2-2: 7-nitro-4-(5-piperidinopentyl)-3,4-dihydro-1*H*-quinoxalin-2-one hydrobromide; VAM2-3: 4-(5-azepanylpentyl)-7-nitro–3,4-dihydro-1*H*-quinoxalin-2-one hydrobromide; VAM2-4: 7-nitro-4-[5-(1,2,3,4-tetrahydroisoquinolin-2-yl)pentyl]-3,4-dihydro-1*H*-quinoxalin-2-one hydrobromide; VAM2-9: 4-[5-(dimethylamino)pentyl]-7-nitro-3,4-dihydro-1*H*-quinoxalin-2-one hydrobromide; VAM2-5: 1-methyl-7-nitro-4-(5-pyrrolidinopentyl)-3,4-dihydro-1*H*-quinoxalin-2-one hydrobromide; VAM2-6: 1-methyl-7-nitro-4-(5-piperidinopentyl)-3,4-dihydro-1*H*-quinoxalin-2-one hydrobromide; VAM2-7: 4-(5-azepanylpentyl)-1-methyl-7-nitro–3,4-dihydro-1*H*-quinoxalin-2-one hydrobromide; VAM2-8: 1-methyl-7-nitro-4-[5-(1,2,3,4-tetrahydroisoquinolin-2-yl)pentyl]-3,4-dihydro-1*H*-quinoxalin-2-one hydrobromide; VAM2-10: 4-[5-(dimethylamino)pentyl]-1-methyl-7-nitro-3,4-dihydro-1*H*-quinoxalin-2-one hydrobromide.

Dimethyl sulfoxide (DMSO - spectroscopy grade) and tetrabutylammonium perchlorate (TBAP), used as supporting electrolyte, were supplied from Fluka.

2.2. Cyclic voltammetry

Cyclic voltammetry (CV) was carried out using a Metrohm 693 VA instrument with a 694 VA Stand convertor and a 693 VA Processor in DMSO (ca. 1.0×10^{-3} M) under nitrogen atmosphere at room

temperature with TBAP (ca. 0.1 M), using a three-electrode cell. A hanging drop mercury electrode (HDME) was used as the working electrode, a platinum wire as the auxiliary electrode, and saturated calomel (SCE) as the reference electrode.

2.3. Electron spin resonance spectroscopy

2.3.1. Electrochemical behavior

ESR spectra were recorded in the X band (9.85 GHz) using a Bruker ECS 106 spectrometer with a rectangular cavity and 50 kHz field modulation. The hyperfine splitting constants were estimated to be accurate within 0.05 G. The nitroquinoxaline radicals were generated by electrolytic reduction *in situ* at room temperature under the same conditions as for the electrochemical case. ESR spectra of the anion radicals were obtained from the electrolysis solution. The ESR spectra were simulated using the program WINEPR Simphonia 1.25 version.

2.3.2. Biological ESR measurement

ESR assays were done using a microsomal fraction (6 mg protein/mL) obtained from *T. cruzi*, in a reaction medium containing 1 mM NADPH, 100 mM DMPO, in 20 mM phosphate buffer, pH 7.4. The experiments were done after 15 min of incubation at 28 °C with VAM2-4, -7, -8 and -10 with *T. cruzi* microsomal fraction, NADPH and DMPO in an aerobic environment. (8×10^7 cells correspond to 1 mg protein or 12 mg of fresh weight)

2.4. Biological assays

2.4.1. Cytotoxicity

Cytotoxicity assays were performed using the MTT reduction method as described previously [25]. Briefly, 5×10^5 RAW 264.7 cells/mL were incubated at different drug concentrations in RPMI 1640 culture medium (5% bovine fetal serum) at 37 °C in a flat-bottom 96-well plate during 18 h when culture medium was replaced with 100 μL of unsupplemented phenol red free-RPMI. For the experiments with trypomastigotes, 10^7 trypomastigotes were incubated in unsupplemented phenol red free-RPMI, at 37 °C for 24 h. 100 μL of the parasite suspension was extracted and incubated in a flat-bottom 96-well plate. For both experiments, MTT was added at a final concentration of 0.5 mg/mL, incubated at 37 °C for 4 h, and then solubilized with 10% sodium dodecyl sulfate–0.1 mM HCl and incubated overnight. Formazan formation was measured at 570 nm with the reference wavelength at 690 nm in a multiwell reader (Asys Expert Plus©, Austria).

2.4.2. Nephelometry

T. cruzi epimastigotes Dm28c strain, from our own collection were grown at 28 °C in Diamond's monophasic medium, as reported earlier [18] but replacing blood by 4 μM hemin. Fetal calf serum was added to a final concentration of 4%. Compounds dissolved in DMSO (1% final concentration) were added to a suspension of 3×10^6 epimastigotes/mL. Parasite growth was followed by nephelometry for 10 days. From the epimastigote exponential growth curve, the culture growth constant (kc) for each compound concentration treatment and for controls was calculated (regression coefficient >0.9, $P < 0.05$). This constant corresponds to the slope resulting from plotting the natural logarithm (ln) of nephelometric measurement vs. time [18]. IC_{kc50} is the drug concentration needed to reduce the kc in 50% and it was calculated by lineal regression analysis from the kc values and the concentrations were used in the employed concentrations. Reported values are mean of at least three independent experiments

2.5. Theoretical calculations

The VAM2-X's were fully optimized by a different level theory to reach the best degree of exactitude and precision in the calculations and so can realize a fine-prediction of the hyperfine splitting pattern. To obtain the best structure and to find the minimum energy structures with the highest abundance conformer population in the gas phase [26,27] a conformational search was performed using molecular mechanics methods (MMFF) as implemented in Spartan' 04. Then, the best conformer was optimized with AM1 semiempirical method [28] as also implemented in Spartan. The last geometry optimization for each selected conformer was performed by means of density functional theory (DFT) as implemented in the GAUSSIAN' 03 package [29] since it is well known that computational models based on density functional theory (DFT) are particularly suitable for the analysis of magnetic properties for open-shell species [30]. The free radical structures were performed using Becke's three parameter exact exchange functional (B3) [31] combined with gradient corrected correlation functional of Lee–Yang–Parr (LYP) [32] of DFT method (U)B3LYP/6-31 g in vacuum and also with Conductor like Polarizable Continuum Model (C-PCM) solvent methodology, using DMSO as solvent for testing the environment influence on the hyperfine splitting [33,34] in the single-point calculations.

2.6. Molecular modeling

2.6.1. Autodock methodologies

Autodock3.0.5 [35] with Lamarckian Genetic Algorithm (LGA) was used to generate the starting complexes. The parameters used for the global search were an initial population of 150 individuals, with a maximal number of energy evaluations of 15,000,000 and a maximal number of generations of 50,000 as end criterion. An elitism value of 1 was used, and a probability of mutation and crossing-over of 0.02 and 0.08 respectively. From the best solutions obtained according to these parameters, some of them defined by the users as the best probabilities, in our case 0.06, were further refined by a local search method such as pseudo Solis and Wets 'PSW'.

The following procedure was employed on the TR docking simulations: 200 runs were done for each case. At the end of each run, the solutions were separated into clusters according to their lowest RMSD and the best score value based on a free empiric energy function. Cluster solutions whose average score was not over 1 kcal mol^{-1} with respect to the best energy obtained from the respective solution were selected. The output of the program delivers two energy values associated with the affinity of the system called final docking energy that corresponds to the amount of energy of intermolecular interaction (ΔG_b) and the energy change after ligand binding to be associated with score of each complex, and the other associated with the free energy of interaction ($\Delta G_{observed}$) that is the sum of the intermolecular interaction energy and the free energy product of the torsion associated with the ligand.

2.6.2. Modeling in trypanothione reductase

The compounds VAM2-X were fully optimized as aforementioned with Gaussian® 03 using the hybrid B3LYP, using electrostatic charge type through single point calculations. The trypanothione reductase (TR) model (based on the crystallographic structure) was downloaded from Protein Data Base, whose code is 1AOG. Refinement and assignation of hydrogens (to pH = 7.0) was realized with YASARA. AMBER charges were assigned to TR through PDB2PQR. *Autodock* defines the conformational space implementing grids all over the space of the possible solutions. With the aim of testing the ability of *Autodock* to converge into

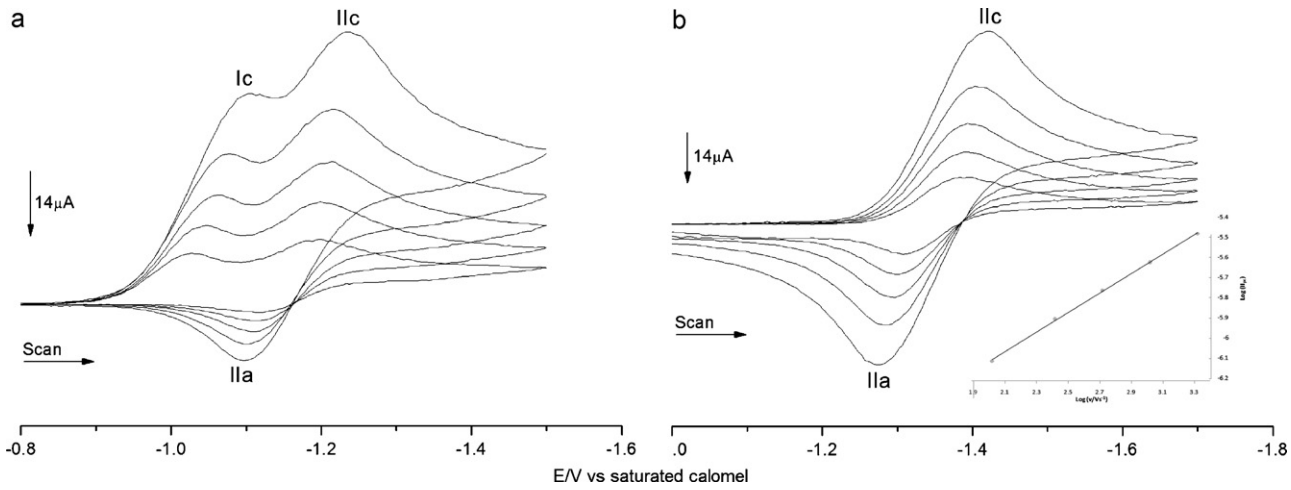

Fig. 2. (a) Cyclic voltammograms of the VAM2-3(1 mM) derivative in aprotic medium (DMSO + 0.1 M TBAP) and at different sweep rates (between 100 and 2000 mV s^{-1}) and (b), the isolated $RNO_2^-/RNO_2^{\bullet-}$ couple of VAM2-3 (1 mM) derivative. Inset within (b): The cathodic peak current vs. log (sweep rate).

solutions that are inside the TR model herein, we have defined a grid of 126 points per grid point in the coordinates *X*, *Y* and *Z* with 0.28 Å of spacing between them, in such a way that all around the catalytic site is covered.

3. Results and discussion

3.1. Cyclic voltammetry

The electrochemical study showed two reduction mechanisms for this quinoxaline family in aprotic medium (DMSO). For those compounds containing a labile hydrogen (A series), two reduction waves appeared (Fig. 2a); one cathodic peak (Ic) around −1.10 V corresponding to the nitro-anion radical $RNO_2^{\cdot-}$ generation and a new wave at higher cathodic potential peak (IIc/IIa, around −1.20 V to −1.30 V, depending on the derivative) corresponding to the electroreduction of the anion $-RNO_2$ (E2), specie generated through a self-protonation reactions (C1) by means of mono-electronic transference. This self-protonation process corresponds to acid–base equilibrium in aprotic media, a typical behavior displayed by nitro-compounds with acidic moieties in their structure [36–38], phenomenon that was corroborated with the application of increasing amounts of NaOH(0.1 M) when going from 0 to 1 mM to obtain only the quasi-reversible wave (Fig. 2b) corresponding to the reduction of the nitro anion to its radical form like dianion radical.

A variation in the potentials (toward negative values) and current peaks occurs when the direct reduction of $-RNO_2$ (from deprotonated specie) is measured, showing only IIc/IIa wave in the voltammograms (Fig. 2b); these variations show that the system reaches a higher degree of reversibility (from relation IIpa/IIpc, giving values close to one) for this one-electron transfer. It is likely that the high negative potential (IIc/IIa wave) of the A deprotonated derivative (Tables 1a and 1b), corresponds to the decrease of the capacity to accept electrons due to its negative net charge.

The dependence of the cathodic peak current, IIpc, with the sweep rate, shows a linear profile with a slope of 0.483 (graph in Fig. 2b) indicating that the electron reversible transference corresponds to a diffusion controlled process without adsorption interference. The self-protonation mechanism is described schematically in Fig. 3.

The compounds of the B series displayed similar cyclic voltammograms, but with different behaviors in their reduction mechanism; the compounds follow the classic mechanism described for nitro compounds in aprotic media or in the presence of inhibitors [38], displaying two waves: the first one corresponds to the nitro radical generation (RNO_2^-) through a one-electronic reduction (E1), and the second, corresponds to the three electrons transfer yielding the respective hydroxylamine derivative (E2), extensively described in the literature [36–38].

Table 1a
Electrochemical parameters without NaOH treatment.

Derivative	$E_{(pIc)}$ (V)	$E_{(pIIc)}$ (V)	$E_{(pIIa)}$ (V)	i_{IIpa}/i_{IIpc}	ΔE (V)	$E_{1/2}$ (V)
VAM2-1	−1.11	−1.23	−1.10	0.21	−0.13	−1.17
VAM2-2	−1.10	−1.25	−1.12	0.26	−0.13	−1.19
VAM2-3	−1.10	−1.22	−1.11	0.21	−0.11	−1.17
VAM2-4	−1.10	−1.30	−1.09	0.31	−0.21	−1.20
VAM2-9	−1.18	−1.38	−1.11	0.25	−0.27	−1.25
VAM2-5	−1.09	−1.17	−1.07	0.23	−0.10	−1.12
VAM2-6	−1.10	−1.21	−1.09	0.24	−0.12	−1.15
VAM2-7	−1.11	−1.26	−1.08	0.31	−0.18	−1.17
VAM2-8	−1.07	−1.32	−1.08	0.32	−0.24	−1.20
VAM2-10	−1.10	−1.27	−1.07	0.30	−0.20	−1.17

$$R\text{-}NO_2 + e^- \rightarrow R\text{-}NO_2^{\bullet-} \quad (E1)$$

$$R\text{-}NO_2^{\bullet-} + 3e^- + 4H^+ \rightarrow R\text{-}NHOH \quad (E2)$$

The reduction potential for both series, with a value near to −1.10 V for the nitro anion radical generation (similar to the 5-indazoles [13,14]) makes entirely feasible to think that these nitroquinoxalines could be reduced in biological conditions as well as the active nitrocompounds aforementioned and so generate oxidative stress.

3.2. ESR spectroscopy

Nitroquinoxaline free radicals were characterized by ESR spectroscopy; they were generated by electrochemical reductions *in situ* in DMSO as solvent by applying the potential corresponding to peak Ic obtained from the CV experiments. The interpretation of the ESR spectra was made through a simulation process which

Table 1b
Electrochemical parameters with NaOH treatment.

Derivative	$E_{(pIIc)}$ (V)	$E_{(pIIa)}$ (V)	i_{IIpa}/i_{IIpc}	ΔE (V)	$E_{1/2}$ (V)
VAM2-1	−1.42	−1.27	0.73	−0.15	−1.35
VAM2-2	−1.44	−1.32	0.73	−0.12	−1.38
VAM2-3	−1.41	−1.29	0.72	−0.12	−1.35
VAM2-4	−1.46	−1.24	0.72	−0.22	−1.35
VAM2-9	−1.49	−1.27	0.64	−0.22	−1.38

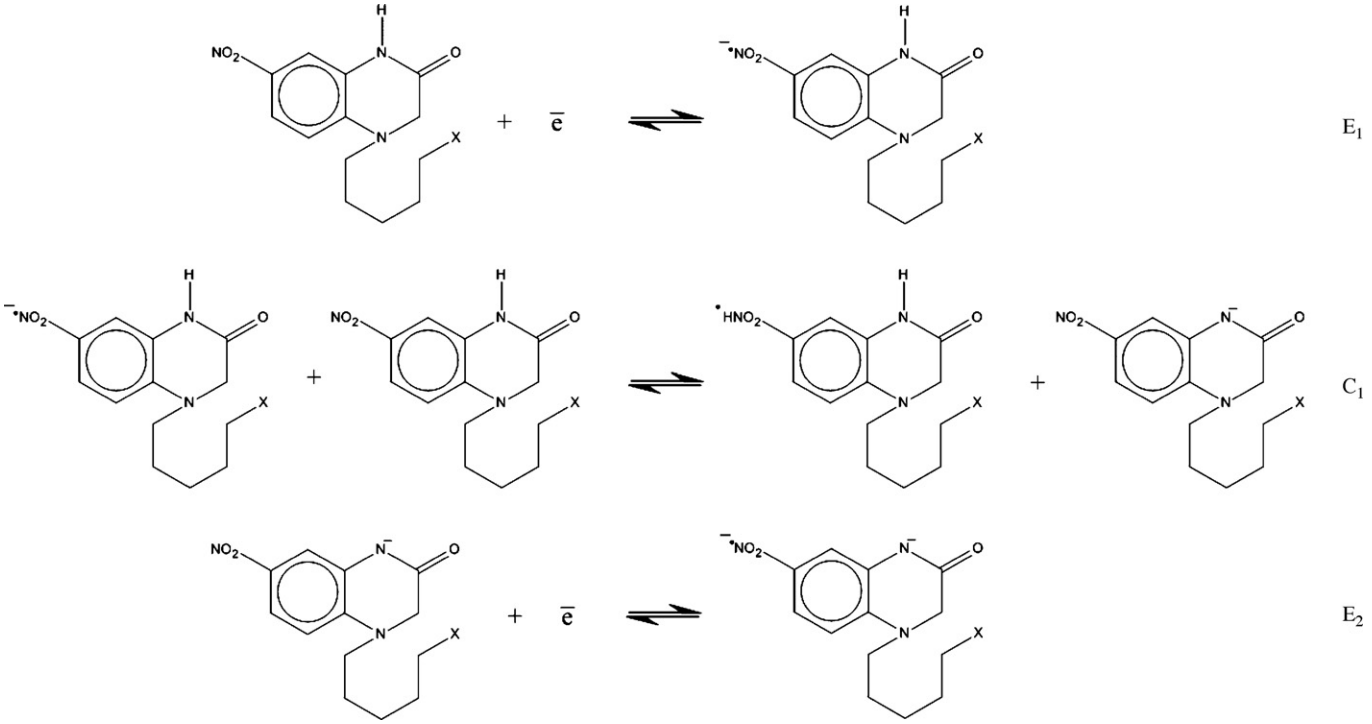

Fig. 3. Self-protonation mechanism proposed for the nitro derivatives of the A series.

confirmed the stability of these radical species due to the delocalization of the unpaired electron. The simulation of the spectra was made using hyperfine coupling constants (hfcc) obtained experimentally, modifying the line width, modulation amplitude and Lorentzian/Gaussian component in the shape of line, until the resulting spectra reached the greatest similarity with the experimental ones. Table 2 presents the hfcc obtained for VAM2-1, and VAM2-5 free radicals, with which were simulated the respective experimental spectra (Fig. 4).

Free radicals of A and B series showed similar spectra, suggesting an analogous behavior for these radicals. Hyperfine pattern proposed for this family corresponds to two triplets of nitrogen: the first assigned to the nitrogen from the nitro group and the second to N-4′, besides six doublets assigned to the hydrogens H-3, -5, -6, -8, -1′ and -2′. The hfcc magnitude, gives a measure of the spin density distribution of the unpaired electron in the molecule, herein case, mainly localized in the nitro group and benzene ring, but also is distributed and extending toward N-4 and H-3 (but in less degree) of the pyrazine ring from quinoxaline molecule, to finally reach part of aliphatic chain (R^2 substituent). We must emphasize the stability of these free radicals caused by the extension of the delocalization of the unpaired electron toward the aliphatic chain, especially when it is compared with other previously studied heterocycles [14] that do not exhibit the degree of delocalization that show the molecules studied in this paper.

In order to corroborate the hyperfine pattern proposed, we have theoretically estimated the hyperfine coupling constants through theoretical calculations (Tables 3 and 4). We have used a methodology extensively used for the calculation of structures of open-shell like free radicals. Thus, starting from the theoretical calculation, we have observed that the experimental hyperfine pattern is in complete agreement with the theoretical estimations. The highest coupling is on the nitrogen from nitro group. Besides the doublets correspond to the hydrogens closest to the nitro group (H-8, H-6 and H-5). Furthermore, as we can see in Fig. 5, the spin density is oriented to the N-4 to reach part of aliphatic chain, which is evidenced by the clear spin density over the H-3 and N-4. Finally, the lowest hyperfine coupling it is easily measurement from ESR spectra, and this is assigned to H-1′ since the calculations did not show spin density of the unpaired electron close to N-1 or H-1 but yes toward the hydrogen in position 1′.

Thus, the simulation of the spectra at the low-field in terms of the numbers of lines, intensity and linewidths of them are in agreement with experimental spectra. However, the experimental spectra showed a remarkable anisotropy in the high field, manifesting the effects of linewidth produced by the interaction between the solvent and the radical, causing anisotropy in the *g* and hyperfine tensors, effects that this kind of calculation is not capable to reproduce, but despite this, we have obtained an accurate perspective of the hyperfine splitting over the molecule.

3.3. Biological assays

In order to evaluate the antiparasitic activity of these compounds, we carried out *in vitro* assays in different cellular models: RAW 264.7 cells, a mammal model, and *Trypanosoma cruzi* trypomastigotes (Dm28c clone) and epimastigotes (Dm28c clone). The concentration where RAW cell viability is reduced in a 50% (IC_{50}) was determined. Similarly, the percentage of viable parasites at a fixed concentration of 20 μM was also determined. Nifurtimox and benznidazole were used as positive controls. 20 μM was chosen because it is the reported nifurtimox IC_{50} concentration for *T. cruzi*

Table 2
Hyperfine coupling constants and *g* value (in Gauss units) of the simulated nitroquinoxaline free radical spectrum.

Radical	N(NO_2)	N-4	H-8	H-6	H-5	H-3	H-1′	H-2′	*g*
VAM2-1	12.100	1.250	3.400	3.600	1.000	0.537	0.537	0.537	2.0126
VAM2-5	11.960	1.150	3.400	3.800	1.700	0.539	0.539	–	2.0110

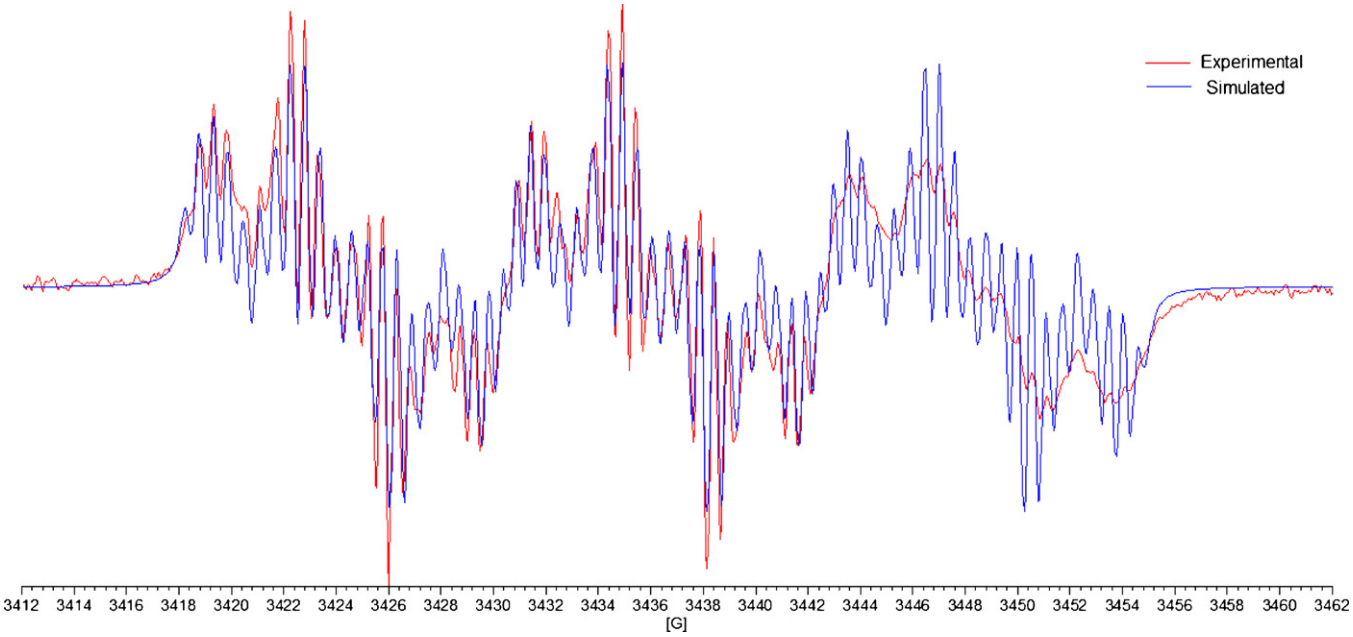

Fig. 4. Experimental and simulated ESR spectrum of VAM2-1 (1 mM) nitro-anion free radical in DMSO. Spectrometer conditions: microwave frequency, 9.68 GHz; microwave power, 20 mW; modulation amplitude, 0.20 G; time constant, 81.92 mS. The spectra were simulated using the following parameters: line width = 0.3 G, Lorentzian/Gaussian ratio = 0.

Dm28c clone [24]. As is shown in Table 5, VAM2-4, VAM2-7, VAM2-8 and VAM2-10 were the most active compounds against *T. cruzi* trypomastigotes when it were compared with nifurtimox, being VAM2-10 almost as active as nifurtimox. However, only VAM2-4, VAM2-7 and VAM2-8 were more selective than nifurtimox or benznidazole, when the relation RAW 264.7 cell IC_{50}/viable parasites is compared; however, the most part of the compounds that displayed activity against *T. cruzi* they also presented toxicity against the mammal system studied. The assays on the epimastigote form displayed lower activities than those of nifurtimox, and only VAM2-8 showed activity relatively close to benznidazole for the epimastigote form.

In order to investigate the capacity of these compounds to generate free radicals into the parasite we incubated our derivatives with *T. cruzi* microsomes in the presence of NADPH, and the spin trapping DMPO [16]. The ESR spectrum obtained when DMPO was added to the system VAM-X compound—*T. cruzi* microsomes, did not show any radical species (data not shown). These results could be indicating that the mode of action of these derivatives is not through reactive species like Nfx, that trigger the superoxide, hydroxyl radical or hydrogen peroxide generation [3,4]. Moreover, there was evidenced that the presence of VAM2-X could not be reduced to other reactive metabolites inside the parasite, which gives us some evidence that the trypanocidal activity of these compounds is not through a mechanism of action such as benznidazole [5].

3.4. Molecular modeling

As mentioned above, Nfx and Bnz work by means of an initial bio-reduction of the NO_2 group (but by following different mechanisms of action) [9], generating a series of reduced metabolites of high toxicity which cause oxidative stress in the parasite. As is well known, the defense of the parasite to the redox imbalance is through an exclusive enzyme (trypanothione reductase, TR), which in its reduced form catalyses the regeneration of trypanothione

Table 3
Hyperfine coupling constants for VAM2-1 free radical (in Gauss units).

Method[a]	N(nitro)	N-4	H-8	H-6	H-5	H-3	H-1′
UB3LYP/6-31G	10.57625	1.34558	3.82637	4.09401	1.53053	1.45427	0.84999
UB3LYP/6-31+G	12.45486	1.49746	3.52398	3.82037	1.30165	1.74710	0.90997
UB3LYP/6-31++G	12.75930	1.47918	3.65479	3.92503	1.42795	1.75655	0.91043
UB3LYP/6-31++G(d.p)	9.75240	1.31058	3.29244	3.57363	1.12015	1.60598	0.87505
Experimental	12.100	1.250	3.400	3.600	1.000	0.537	0.537

[a] Single-point calculations with the C-PCM solvation model.

Table 4
Hyperfine coupling constants for VAM2-5 free radical (in Gauss units).

Method[a]	N(nitro)	N-4	H-8	H-6	H-5	H-3	H-1′
UB3LYP/6-31G	10.58037	1.11209	3.67827	4.11448	1.52165	1.28703	1.84565
UB3LYP/6-31+G	12.96304	1.25942	3.66589	4.07415	1.55283	1.61622	1.94029
UB3LYP/6-31++G	12.95613	1.26105	3.65517	4.06614	1.54896	1.61765	1.93966
UB3LYP/6-31++G(d.p)	10.30838	1.08400	3.42503	3.83682	1.38224	1.47096	1.86430
Experimental	11.960	1.150	3.400	3.800	1.700	0.539	0.539

[a] Single-point calculations with the C-PCM solvation model.

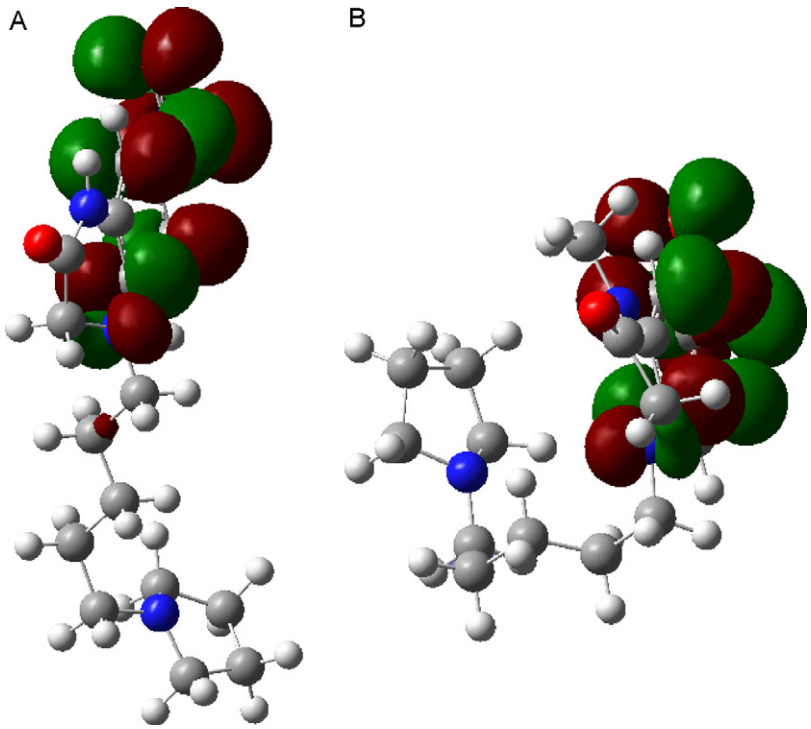

Fig. 5. Spin density of the unpaired electron. (A) VAM2-1 and (B) VAM2-5 free radicals.

disulfide ($T[S]_2$) to trypanothione ($T[SH]_2$) (a low molecular-weight thiol able to inactivate free radicals) and is also responsible for maintaining a reduced environment essential to the survival of the parasite [5,39].

Trypanothion reductase is a homodimeric enzyme FAD depending on two NADH binding sites and two catalytic binding sites for $T[S]_2$ placed between the subunits interface. The binding mode of $T[S]_2$ in the catalytic site is in such a way that one of the γGlu-Cys-Gly chains is near the catalytic machinery formed by Cys^{53}, Cys^{58} and His^{461} (according to the pdb structure 1BZL [40]). The interaction between the enzyme and endogen substrate, is frequently used as target to the design of new drugs [26,41,42]. In this sense, several factors of significance in the interaction of the substrate with the enzyme, such as the charge of –NH– group placed into the spermidine chain [43] and the orientation of this latter into the catalytic site have been reported, besides factors such as the size of cavity and the hydrophobic character of the same. The aim of this case is to check by means of molecular modeling studies if our compounds are capable of inhibiting TR through this pathway.

In order to evaluate a different action mechanism we have studied the affinity of VAM2-X like substrate of TR. The results of the docking studies show on the one part that the A and B series have different behaviors when they are included in the catalytic site of TR; the B series showed inauspicious docking energies (ca. −8 kcal/mol), well below the docking energy of trypanothione–TR complex as well as its location in the enzyme, far from the catalytic site, unlike the A series that was placed near the catalytic site besides auspicious docking energies. The differences observed would be explained in terms of the substituent in R^1 position, e.g., the methyl group (exclusive of the B series) sited in R^1 position confers a larger hydrophobicity to the molecule, unlike the A series that carries in their structure a hydrogen of acid character (in R^1-position) by promoting an increase in the electrostatic interaction. The observed behavior indicates that this group might be behaving like a bioisostere of the amino group of the spermidine chain from trypanothione disulfide. The hydrogen acid (from A series exclusively) is not found into the compounds of the B series, which could explain the low affinity of the B series to the catalytic site. Thus, in consequence, we have discarded the B series as poten-

Table 5
Cytotoxicity and trypanocidal activity.

Compound	IC_{50} (μM) (RAW cells)	Viable parasites[a] (% of control) (trypomastigote)	IC_{50} (μM) (epimastigote)
VAM2-1	226.1 ± 19.4	93.3 ± 7.7	–
VAM2-2	175.9 ± 14.3	81.5 ± 5.5	–
VAM2-3	162.1 ± 53.4	74.1 ± 1	–
VAM2-4	35.8 ± 1.2	2.3 ± 3.1	79.76 ± 10.22
VAM2-5	117.5 ± 7.3	95.12 ± 5.9	–
VAM2-6	136.0 ± 14.2	67.6 ± 12.2	–
VAM2-7	67.8 ± 3.2	0.6 ± 1.7	85.26 ± 10.69
VAM2-8	163.2 ± 2	2.4 ± 6.1	50.20 ± 2.17
VAM2-9	133.0 ± 29.1	86.9 ± 8.6	–
VAM2-10	152.8 ± 30.3	39.6 ± 7.8	110.51 ± 244.6
Nifurtimox	227.7 ± 2.5	25.6 ± 3.9	14.01 ± 1.75[b]
Benznidazole	105.9 ± 22.7	66.7 ± 2.8	43.64 ± 1.59[b]

[a] Viable parasites at 20 μM dose of each compound tested.
[b] From Ref. [24].

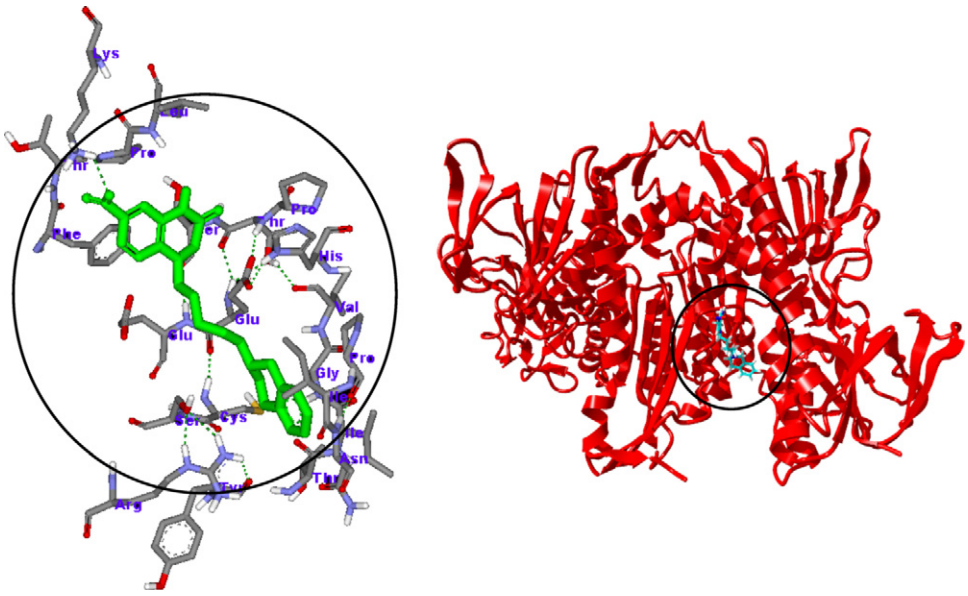

Fig. 6. Interaction mode of VAM2-4–TR complex: the figure displays the conformational mode of the compound VAM2-4 (with only one color for more clearness). It is observable the interaction between the nitro group and Lis^{402} and the inclination of the nitro group in respect of the aromatic ring plane.

Table 6
Docking parameters of the nitroquinoxaline–TR and trypanothione–TR complexes[a].

Compound	*E*(docking)	*E*(binding)	K_i	*E*(int-lig)
VAM2-1	−12.01	−14.56	2.13E−11	2.55
VAM2-2	−12.38	−14.67	1.77E−11	2.29
VAM2-3	−12.81	−14.91	1.17E−11	2.10
VAM2-4	−14.56	−17.18	2.54E−13	2.62
VAM2-9	−13.93	−14.17	4.08E−11	0.24
$T[S]_2$	−13.68	−9.94	5.15E−08	0.00

[a] Energies (*E*(*x*)) and inhibition constants (K_i) in kcal/mol and mol/L units respectively.

tials inhibitors of TR (all docking parameters are summarized in Table 6).

For compounds potentially capable to inhibit TR (A series), two conformational modes were found in the surrounding of the catalytic site by showing dependence with the cyclic moiety located at the end of the aliphatic chain which is described by means of their interaction modes as follows:

VAM2-1 was the first compound docked: the interaction mode takes place when the nitroheterocycle ring is located in the hydrophobic cavity formed by the Gly^{57}, Lys^{61}, Phe^{183}, Phe^{199}, Ile^{200} and Leu^{334}, close to the TR catalytic site, but without interacting with the relevant amino acids of this latter. Thus, due to the shape of the cavity, the ring is tilted slightly over the original plane; moreover, the hydrophobicity of the site forces the ring and the nitro group to maintain its initial planarity into the cavity of the macromolecule without showing specific interactions (hydrogen bonds). The estimated docking energy (a score that we have called "fitness") was of ca. −12.01 kcal/mol; the inhibition constant estimated for this complex is ca. 10^{-11} M. A comparison with the docking energy of the trypanothione–TR complex (ca. −13.68 kcal/mol), shows that the docking energy of VAM2-1 is insufficient to consider this compound like potential TR inhibitor since it does not interact with the appropriate amino acids for the catalytic activity [44,45].

VAM2-2 was placed like VAM2-1, although it was oriented in opposite position (relative to VAM2-1) into the cavity by showing one interaction by hydrogen bond near 1.75 Å between a hydrogen (from ammonium group of Lis^{61}) and one of the oxygen from nitro group; the assigned fitness to this compound is of ca. −12.38 kcal/mol, insufficient to consider it like a potential inhibitor. In this way, a similar conformational mode for VAM2-3 was found, however, as in the previous cases with a low fitness to act as an inhibitor of TR.

In the case of VAM2-4 (biologically active), the main difference between the other compounds of this family is its tetrahydroisoquinolyl moiety (X = THIQ) placed at the last part of the aliphatic chain; with large volume, relative planarity and high non-polar properties that hinder its insertion in small cavities unlike the previous cases. This molecule is located exactly in the catalytic site because the THIQ substituent does not allow the passage to a smaller and slightly polar zone as in the case of VAM2-1, -2 and -3. Thus, VAM2-4 interacts with the most part of the amino acids involved in the catalysis, among them His^{461} and Glu^{466}, which are crucial for the catalytic activity of TR evidencing a hydrogen bond interaction between ammonium group from Lis^{402} with one of the oxygens from nitro group, the latter tilted ca. 90° in relation to the plane of the quinoxaline ring. The docking fitness for this complex is ca. −14.56 kcal/mol, auspicious value compared with the trypanothione–TR complex, which allows us to propose VAM2-4 as a potential TR inhibitor. The conformational mode model is represented in Fig. 6.

VAM2-9 showed a favorable score to the formation of the complex of ca. −13.93 kcal/mol (better than trypanothione–TR complex), sufficient to consider it as an inhibitor, however this molecule is located away from the catalytic site without interacting with relevant residues of the catalytic machinery. These results could be explained by means of the characteristics of the X substituent, because of its small volume and polarity. Thus, the compound VAM2-9 cannot be proposed as potential inhibitor of TR

4. Conclusions

The electrochemical behavior of two series of nitroquinoxalines is here described; depending on the substituent at R^1-position (H or CH_3) shows two different reduction mechanisms: self-protonation and electrochemical pure respectively. The hyperfine structure of the nitro radical species corresponding to the first wave of CV has been studied by means of ESR spectroscopy, finding an anisotropic

spectrum at entire field and a strong influence of the solvent at high field. Moreover, the *in vitro* assays displayed four new compounds highly toxic against the parasite in its trypomastigote form. Moreover, it was observed that there is no relationship between the redox potential and the biological activities. ESR biological assays showed that these compounds are not related to the mechanisms of Nfx. or Bnz. Finally, the inhibition mechanism of TR was explored by molecular modeling studies. Thus, we have evidenced that one of the possible action modes of VAM2-4, the most active compound against *T. cruzi*, could be through the inhibition of the enzyme trypanothione reductase.

Acknowledgements

This research was supported by FONDECYT (Chile) through the project 1071068 in collaboration with the project CSIC 16/07-08 and by the "*Comisión Interministerial de Ciencia y Tecnología*" (CICYT, Spain) Project SAF2006-04698. B. Aguilera grateful to CONICYT (Chile) - Doctoral fellowship - 21080766.

References

[1] C.J. Schofield, J. Jannin, R. Salvatella, Trends in Parasitology 22 (2006) 583–588.
[2] J.A. Urbina, R. Docampo, Trends in Parasitology 19 (2003) 495–501.
[3] R. Docampo, Chemico-Biological Interactions 73 (1990) 1–27.
[4] R. Docampo, A.O.M. Stoppani, Archives of Biochemistry and Biophysics 197 (1979) 317–321.
[5] J.D. Maya, Y. Repetto, M. AgosIn, J.M. Ojeda, R. Tellez, C. Gaule, A. Morello, Molecular and Biochemical Parasitology 86 (1997) 101–106.
[6] C.M. Sreider, L. Grinblat, A.O.M. Stoppani, Biochemical Pharmacology 40 (1990) 1849–1857.
[7] M.M. de Mecca, S.L. Fanelli, L.C. Bartel, C.R. de Castro, E.G. Díaz, J.A. Castro, Life Sciences 81 (2007) 144–152.
[8] J.A. Castro, M.M. deMecca, L.C. Bartel, Human and Experimental Toxicology 25 (2006) 471–479.
[9] W.H. Koppenol, Free Radical Biology and Medicine 15 (1993) 645–651.
[10] S. Cuzzocrea, D.P. Riley, A.P. Caputi, D. Salvemini, Pharmacological Reviews 53 (2001) 135–159.
[11] J.R. Coura, S.L.d. Castro, Memórias do Instituto Oswaldo Cruz 97 (2002) 3–24.
[12] C. Jullian, J. Morales-Montecinos, G. Zapata-Torres, B. Aguilera, J. Rodriguez, V. Arán, C. Olea-Azar, Bioorganic & Medicinal Chemistry 16 (2008) 5078–5084.
[13] J. Rodríguez, A. Gerpe, G. Aguirre, U. Kemmerling, O.E. Piro, V.J. Arán, J.D. Maya, C. Olea-Azar, M. González, H. Cerecetto, European Journal of Medicinal Chemistry 44 (2009) 1545–1553.
[14] J. Rodríguez, C. Olea-Azar, G. Barriga, C. Folch, A. Gerpe, H. Cerecetto, M. González, Spectrochimica Acta Part A: Molecular and Biomolecular Spectroscopy 70 (2008) 557–563.
[15] V.J. Arán, C. Ochoa, L. Boiani, P. Buccino, H. Cerecetto, A. Gerpe, M. González, D. Montero, J.J. Nogal, A. Gómez-Barrio, A. Azqueta, A. López de Ceráin, O.E. Piro, E.E. Castellano, Bioorganic & Medicinal Chemistry 13 (2005) 3197–3207.
[16] L. Boiani, A. Gerpe, V.J. Arán, S. Torres de Ortiz, E. Serna, N. Vera de Bilbao, L. Sanabria, G. Yaluff, H. Nakayama, A. Rojas de Arias, J.D. Maya, J.A. Morello, H. Cerecetto, M. González, European Journal of Medicinal Chemistry 44 (2009) 1034–1040.
[17] L. Otero, G. Aguirre, L. Boiani, A. Denicola, C. Rigol, C. Olea-Azar, J.D. Maya, A. Morello, M. González, D. Gambino, H. Cerecetto, European Journal of Medicinal Chemistry 41 (2006) 1231–1239.
[18] M. Vieites, L. Otero, D. Santos, C. Olea-Azar, E. Norambuena, G. Aguirre, H. Cerecetto, M. González, U. Kemmerling, A. Morello, J. Diego Maya, D. Gambino, Journal of Inorganic Biochemistry 103 (2009) 411–418.
[19] M. Vieites, L. Otero, D. Santos, J. Toloza, R. Figueroa, E. Norambuena, C. Olea-Azar, G. Aguirre, H. Cerecetto, M. González, A. Morello, J.D. Maya, B. Garat, D. Gambino, Journal of Inorganic Biochemistry 102 (2008) 1033–1043.
[20] Y. Marrero-Ponce, O. Rivera-Borroto, A. Meneses-Marcel, J. Escario, A. Gómez Barrio, V. Arán, M. Martins Alho, D. Montero Pereira, J. Nogal, F. Torrens, F. Ibarra-Velarde, Y. Vera Montenegro, A. Huesca-Guillén, N. Rivera, C. Vogel, QSAR & Combinatorial Science 28 (2009) 9–26.
[21] A. Meneses-Marcel, Y. Marrero-Ponce, Y. Machado-Tugores, A. Montero-Torres, D.M. Pereira, J.A. Escario, J.J. Nogal-Ruiz, C. Ochoa, V.J. Arán, A.R. Martínez-Fernández, R.N. García Sánchez, Bioorganic & Medicinal Chemistry Letters 15 (2005) 3838–3843.
[22] M.A.M. Alho, Y. Marrero-Ponce, A. Meneses-Marcel, Y.M. Tugores, A. Montero-Torres, F. Pérez-Giménez, A. Gómez-Barrio, J.J. Nogal, R.N. García-Sánchez, M.C. Vega, M. Rolón, A.R. Martínez-Fernández, J.A. Escario, N. Rivera, F. Ibarra-Velarde, M. Mondragón, R. Mondragón, R. Chicharro, V.J. Arán, Antiprotozoan lead discovery by aligning dry and wet screening: prediction, synthesis, and biological assay of novel quinoxalinones, in: Proceedings of the 12th International Electronic Conference on Synthetic Organic Chemistry, 2008.
[23] F. Irigoín, L. Cibils, M.A. Comini, S.R. Wilkinson, L. Flohé, R. Radi, Free Radical Biology and Medicine 45 (2008) 733–742.
[24] M. Faundez, L. Pino, P. Letelier, C. Ortiz, R. Lopez, C. Seguel, J. Ferreira, M. Pavani, A. Morello, J.D. Maya, Antimicrob. Agents Chemother. 49 (2005) 126–130.
[25] S. Muelas-Serrano, J.J. Nogal-Ruiz, A. Gómez-Barrio, Parasitology Research 86 (2000) 999–1002.
[26] M.L. Cunningham, M.J.J.M. Zvelebil, A.H. Fairlamb, European Journal of Biochemistry 221 (1994) 285–295.
[27] S. Baillet, E. Buisine, D. Horvath, L. Maes, B. Bonnet, C. Sergheraert, Bioorganic & Medicinal Chemistry 4 (1996) 891–899.
[28] M.J.S. Dewar, E.G. Zoebisch, E.F. Healy, J.J.P. Stewart, Journal of the American Chemical Society 107 (1985) 3902–3909.
[29] M.J. Frisch, G.W. Trucks, H.B. Schlegel, G.E. Scuseria, M.A. Robb, J.R. Cheeseman, V.G. Zakrzewski, J.A. Montgomery, R.E. Stratmann, J.C. Burant, S. Dapprich, J.M. Millam, A.D. Daniels, K.N. Kudin, M.C. Strain, O. Farkas, J. Tomasi, V. Barone, M. Cossi, R. Cammi, B. Mennucci, C. Pomelli, C. Adamo, S. Clifford, J. Ochterski, G.A. Petersson, P.Y. Ayala, Q. Cui, K. Morokuma, N. Rega, P. Salvador, J.J. Dannenberg, D.K. Malick, A.D. Rabuck, K. Raghavachari, J.B. Foresman, J. Cioslowski, J.V. Ortiz, A.G. Baboul, B.B. Stefanov, G. Liu, A. Liashenko, P. Piskorz, I. Komaromi, R. Gomperts, R.L. Martin, D.J. Fox, T. Keith, M.A. Al-Laham, C.Y. Peng, A. Nanayakkara, M. Challacombe, P.M.W. Gill, B. Johnson, W. Chen, M.W. Wong, J.L. Andres, C. Gonzalez, M. Head-Gordon, E.S. Replogle, J.A. Pople, GAUSSIAN' 98. Revision A.11.2 ed., Gaussian Inc., Pittsburgh, PA, 2001.
[30] M. D'Amore, R. Improta, V. Barone, Journal of Physical Chemistry A 107 (2003) 6264–6269.
[31] A.D. Becke, Physical Reviews A 38 (1988) 3098–3100.
[32] C.T. Lee, W.T. Yang, R.G. Parr, Physical Reviews B 37 (1988) 785–789.
[33] V. Barone, M. Cossi, Journal of Physical Chemistry A 102 (1998) 1995–2001.
[34] M. Cossi, V. Barone, R. Cammi, J. Tomasi, Chemical Physical Letters 255 (1996) 327–335.
[35] G.M. Morris, D.S. Goodsell, R.S. Halliday, R. Huey, W.E. Hart, R.K. Belew, A.J. Olson, Journal of Computational Chemistry 19 (1998) 1639–1662.
[36] J.A. Bautista-Martínez, I. González, M. Aguilar-Martínez, Electrochimica Acta 49 (2004) 3403–3411.
[37] S. Bollo, L.J. Núñez-Vergara, M. Bontá, G. Chauviere, J. Périé, J.A. Squella, Journal of Electroanalytical Chemistry 511 (2001) 46–54.
[38] J. Carbajo, S. Bollo, L.J. Núñez-Vergara, A. Campero, J.A. Squella, Journal of Electroanalytical Chemistry 531 (2002) 187–194.
[39] A.H. Fairlamb, A. Cerami, Annual Review of Microbiology 46 (1992) 695–729.
[40] Y. Zhang, C.S. Bond, S. Bailey, M.L. Cunningham, A.H. Fairlamb, W.N. Hunter, Protein Science 5 (1996) 52–61.
[41] G. Aguirre, E. Cabrera, H. Cerecetto, R. Di Maio, M. González, G. Seoane, A. Duffaut, A. Denicola, M.J. Gil, V. Martínez-Merino, European Journal of Medicinal Chemistry 39 (2004) 421–431.
[42] C.S. Bond, Y. Zhang, M. Berriman, M.L. Cunningham, A.H. Fairlamb, W.N. Hunter, Structure 7 (1999) 81–89.
[43] C.H. Faerman, S.N. Savvides, C. Strickland, M.A. Breidenbach, J.A. Ponasik, B. Ganem, D. Ripoll, R. Luise Krauth-Siegel, P. Andrew Karplus, Bioorganic & Medicinal Chemistry 4 (1996) 1247–1253.
[44] B. Bonnet, D. Soullez, E. Davioud-Charvet, V. Landry, D. Horvath, C. Sergheraert, Bioorganic & Medicinal Chemistry 5 (1997) 1249–1256.
[45] M.O.F. Khan, S.E. Austin, C. Chan, H. Yin, D. Marks, S.N. Vaghjiani, H. Kendrick, V. Yardley, S.L. Croft, K.T. Douglas, J. Med. Chem. 43 (2000) 3148–3156.